

## THE FUNDAMENTAL PLANE AT $Z = 1.27$ : FIRST CALIBRATION OF THE MASS SCALE OF RED GALAXIES AT REDSHIFTS $Z > 1$ <sup>1,2</sup>

PIETER G. VAN DOKKUM

California Institute of Technology, MS105-24, Pasadena, CA 91125

AND

S. A. STANFORD<sup>3</sup>

Physics Department, University of California-Davis, Davis, CA 95616

*Accepted for publication in the Astrophysical Journal*

### ABSTRACT

We present results on the Fundamental Plane of early-type galaxies in the cluster RDCS J0848+4453 at  $z = 1.27$ . Internal velocity dispersions of three  $K$ -selected early-type galaxies are determined from deep Keck spectra, using absorption lines in the rest-frame wavelength range 3400 Å – 4000 Å. Structural parameters are determined from *Hubble Space Telescope* NICMOS images. The galaxies show substantial offsets from the Fundamental Plane of the nearby Coma cluster, as expected from passive evolution of their stellar populations. The offsets from the Fundamental Plane can be expressed as offsets in mass-to-light ( $M/L$ ) ratio. The  $M/L$  ratios of the two most massive galaxies are consistent with an extrapolation of results obtained for clusters at  $0.02 < z < 0.83$ . The evolution of early-type galaxies with masses  $> 10^{11} M_{\odot}$  is well described by  $\ln M/L_B \propto (-1.06 \pm 0.09)z$ , corresponding to passive evolution of  $-1.50 \pm 0.13$  magnitudes at  $z = 1.3$ . Ignoring selection effects, the best fitting stellar formation redshift is  $z_* = 2.6^{+0.9}_{-0.4}$  for an  $\Omega_m = 0.3$ ,  $\Omega_{\Lambda} = 0.7$  cosmology and a Salpeter IMF, corresponding to a luminosity weighted age at the epoch of observation of  $\sim 2$  Gyr. The  $M/L$  ratios of these two galaxies are also in excellent agreement with predictions from models that include selection effects caused by morphological evolution (“progenitor bias”). The third galaxy is a factor  $\sim 10$  less massive than the other two, shows strong Balmer absorption lines in its spectrum, and is offset from the Coma Fundamental Plane by 2.9 mag in rest-frame  $B$ . Larger samples are required to determine whether such young early-type galaxies are common in high redshift clusters. Despite their large range in  $M/L$  ratios, all three galaxies fall in the “Extremely Red Object” (ERO) class with  $I - H > 3$  and  $R - K > 5$ , and our results show that it is hazardous to use simple models for converting luminosity to mass for these objects. The work presented here, and previous mass measurements at lower redshift, can be considered first steps to empirically disentangle luminosity and mass evolution at the high mass end of the galaxy population, lifting an important degeneracy in the interpretation of evolution of the luminosity function.

*Subject headings:* galaxies: clusters: general — galaxies: evolution — galaxies: structure of — galaxies: kinematics and dynamics — galaxies: elliptical and lenticular, cD

### 1. INTRODUCTION

One of the defining characteristics of galaxy formation models is the evolution of the galaxy mass function with time. In traditional “monolithic collapse” models, galaxies formed at early times from the collapse of proto-galactic gas clouds, and the mass function evolved very little after  $z \sim 3$  (e.g., Eggen, Lynden-Bell, & Sandage 1962; Searle, Sargent, & Bagnuolo 1973; Jimenez et al. 1999). In contrast, hierarchical models for galaxy formation in Cold Dark Matter cosmologies postulate that galaxies continuously form in mergers, implying strong evolution in the mass function over the redshift range  $0 < z < 2$  (e.g., White & Frenk 1991; Kauffmann & Charlot 1998; Cole et al. 2000; Somerville, Primack, & Faber 2001).

Although these models are very different, determining which is closer to reality has proven to be quite difficult. An important constraint on the evolution of the mass function is the evolution of the  $K$ -band luminosity function, under the assumption that  $K$ -band light is a good tracer of stellar mass to  $z \gtrsim 1$  (Kauffmann & Charlot 1998). Observationally, this evolution is difficult to measure as deep  $K$ -selected redshift surveys over large

fields are required. Past and ongoing surveys seem to indicate some evolution in the number density, although the amount is still uncertain (e.g., Cowie et al. 1996; Kauffmann & Charlot 1998; Stern et al. 2001; Drory et al. 2001; Cimatti et al. 2002). Other studies focus exclusively on the reddest galaxies, usually defined as having  $I - H > 3$  or  $R - K > 5$  (e.g., Daddi, Cimatti, & Renzini 2000; McCarthy et al. 2001; Roche et al. 2002). A large fraction of these “Extremely Red Objects” (EROs) are thought to be passively evolving massive galaxies at  $1 \lesssim z \lesssim 2$ , whose number density may constrain the evolution of the mass function without the need for full redshift information.

One of the main uncertainties in the interpretation is the model-dependent conversion of luminosity to stellar mass. The observed evolution of the luminosity function is caused by a combination of evolution of the underlying mass function and the evolution of stellar populations. At  $z \sim 1$ , the  $K$ -band samples the rest-frame  $J$ -band, and mass-to-light ( $M/L$ ) ratios of galaxies are quite uncertain even if they are “pre-selected” to be passively evolving through the use of broad-band colors. As

<sup>1</sup> Based on observations with the NASA/ESA *Hubble Space Telescope*, obtained at the Space Telescope Science Institute, which is operated by AURA, Inc., under NASA contract NAS 5-26555.

<sup>2</sup> Based on observations obtained at the W. M. Keck Observatory, which is operated jointly by the California Institute of Technology and the University of California.

<sup>3</sup> Institute of Geophysics and Planetary Physics, Lawrence Livermore National Laboratory

an example, the Worthey (1994) models<sup>4</sup> predict a variation of a factor 2.4 in the  $M/L_J$  ratio for luminosity weighted ages ranging from 1 – 5 Gyr and [Fe/H] ranging from  $-0.225$  to  $+0.5$ . At the bright end of the luminosity function this uncertainty in  $M/L$  ratio contributes directly to the uncertainty in the number density.

For a correct interpretation of the luminosity function it is therefore essential to measure masses and mass-to-light ratios directly, so that luminosities can be converted to masses in a model-independent way. Total masses of galaxies are notoriously difficult to measure, but scaling relations such as the Tully-Fisher relation for spiral galaxies (Tully & Fisher 1977) and the Fundamental Plane (FP) for early-type galaxies (Djorgovski & Davis 1987; Dressler et al. 1987) can be used to constrain the evolution of the  $M/L$  ratio relative to local samples (see Franx 1993).

In star forming disks aging of the stellar population is compensated by the formation of new stars, and models predict only modest or even negative evolution in the  $M/L$  ratio with time (e.g., Pozzetti, Bruzual A., & Zamorani 1996; Ferreras & Silk 2001). The observed evolution of the Tully-Fisher relation lends support to these models, ruling out strong (1–2 mag) evolution over the redshift range  $0 < z < 1.3$ , at least for the most massive galaxies (Vogt et al. 1996, 1997; van Dokkum & Stanford 2001; Ziegler et al. 2002).

By contrast, the  $M/L$  ratios of early-type galaxies (and the bulges of spiral galaxies) are expected to increase over time, as the demise of massive stars causes their stellar populations to fade (Tinsley & Gunn 1976). The evolution of  $M/L$  ratios of early-type galaxies has been measured in rich clusters at  $0.02 \leq z \leq 0.83$  (e.g., van Dokkum & Franx 1996; Kelson et al. 1997; Bender et al. 1998; van Dokkum et al. 1998), and in the general field to  $z \approx 0.7$  (Treu et al. 1999; van Dokkum et al. 2001a; Treu et al. 2002), using the Fundamental Plane relation. The cluster data show a gradual increase of the mean  $M/L_B$  ratio by a factor  $\sim 3$  since  $z = 0.83$  (for  $\Omega_m = 0.3$ ,  $\Omega_\Lambda = 0.7$ ). The results for the general field are still somewhat uncertain, but indicate that field early-type galaxies have similar  $M/L$  ratios as those in clusters, at least out to  $z \approx 0.6$ .

In this paper, we present results on the Fundamental Plane and  $M/L$  ratios in the cluster RDCS J0848+4453 at  $z = 1.27$  (Stanford et al. 1997), probably the highest redshift accessible for velocity dispersion measurements with the current generation of telescopes. Although it is hazardous to extrapolate the results presented here to the general population of distant red galaxies, studies of the Tully-Fisher relation and the FP at  $z \gtrsim 1$  can be regarded as tentative first steps toward an empirical determination of the mass function at high redshift. We assume  $\Omega_m = 0.3$  and  $\Omega_\Lambda = 0.7$  throughout. We used  $H_0 = 50 \text{ km s}^{-1} \text{ Mpc}^{-1}$  where needed, but note that our results are not dependent on the value of the Hubble constant.

## 2. SPECTROSCOPY

### 2.1. Sample Selection and Observations

The sample selection was based on an extensive  $BRIzJK_s$  survey of a 28 arcmin<sup>2</sup> field in Lynx (Eisenhardt et al., in preparation). Keck spectroscopy and Chandra imaging (Stanford et al. 2001) has revealed that the Lynx field contains three distant X-ray clusters: RDCS J0848+4452 at  $z = 0.57$  (Holden et al. 2001), RDCS J0848+4456 at  $z = 1.26$  (Rosati et al. 1999), and

RDCS J0848+4453 at  $z = 1.27$  (Stanford et al. 1997). Galaxies in the Lynx field were selected on the basis of their  $K_s$  magnitude. Three multislit masks were designed. The primary sample consists of seven  $K_s < 19$  galaxies with spectroscopic redshifts  $1.25 < z < 1.29$ ; these galaxies were repeated in each mask. Remaining space in the three masks was filled with  $K_s < 20$  galaxies without spectroscopic redshift.

The Lynx field was observed on 2001 January 20–21 with the Low Resolution Imaging Spectrograph (LRIS; Oke et al. 1995) on the Keck II Telescope. The D680 dichroic was used, in conjunction with the 600 lines  $\text{mm}^{-1}$  grating blazed at  $1 \mu\text{m}$  in the red and the 300 lines  $\text{mm}^{-1}$  grism blazed at  $5000 \text{ \AA}$  in the blue. The  $1''/2$  wide slits give a resolution of  $5.7 \text{ \AA}$  FWHM as measured from the width of atmospheric emission lines, which corresponds to  $\sigma_{\text{instr}} \approx 80 \text{ km s}^{-1}$  at  $9000 \text{ \AA}$ . Conditions were photometric, and the seeing was  $\approx 0''/9$ . In order to facilitate sky subtraction the galaxies were moved along the slit between successive exposures, with offsets  $-1''/5$ ,  $-4''/5$ ,  $+1''/5$ ,  $+4''/5$  with respect to the initial position. The integration time for each exposure was 1800 s. Each of the three masks was observed for a total of 14.4 ks, split in two sequences of the four dither positions. The total integration time for galaxies in the primary sample is 43.2 ks, or twelve hours.

Initial results from our deep spectroscopy were presented in van Dokkum & Stanford (2001). The present paper discusses the three galaxies in the primary sample that fall within the area of our deep *Hubble Space Telescope* (*HST*) WFPC2 and NICMOS imaging of RDCS J0848+4453 at  $z = 1.27$ . They are the brightest, second brightest, and fourth brightest early-type galaxies in our  $K$ -selected sample of cluster galaxies observed with *HST* (van Dokkum et al. 2001b).

### 2.2. Reduction

Each set of four dithered 1800 s exposures was reduced separately. Each slitlet was treated as a separate, long slit spectrum. Bias was subtracted by fitting low order polynomials to the overscan regions. The red CCD was read out using two amplifiers; the overscan region for each amplifier was fitted separately. No systematic variations are present in the residuals of bias frames or the overscan regions of science images.

The most critical step in the data reduction is the removal of the fringe pattern in the red exposures. Internal flatfields were taken every  $\sim 90$  minutes, such that there was a flatfield within one hour of each science exposure. For each slit, the flatfield was divided by the average response in the wavelength direction. The response was obtained by averaging the flatfield in the spatial direction and fitting a fifth order polynomial in the wavelength direction. Flatfielding reduced the peak-to-peak variation in the fringe pattern from  $\approx 7\%$  to  $\approx 2\%$ . A map of the residual fringe pattern was created from the four dithered exposures in the following way. First, sky lines were fitted by a third order polynomial, masking the galaxy spectrum (and any other objects) in the fit. Next, the median of the four sky subtracted spectra was computed, disregarding pixels at the positions of object spectra. Finally, this median residual map was fitted by a low order polynomial in the wavelength direction to remove faint unmasked objects and any residuals from galaxy spectra. The fringe map was subtracted from each of the four exposures. Residual peak-to-peak variations are  $< 0.5\%$ , and the noise in the final combined spectra is dominated by Poisson fluctuations.

<sup>4</sup> [www.astro.wsu.edu/worthey/dial/dial\\_a\\_model.html](http://www.astro.wsu.edu/worthey/dial/dial_a_model.html)

Cosmic ray removal is not straightforward, despite the large number of independent exposures. As a result of our dithering procedure and flexure in the spectrograph the positions of galaxy spectra as well as those of sky lines change from one exposure to the next. Therefore, the sky lines and object spectra were modeled and subtracted before identifying cosmic rays in the residual images. Sky lines were modeled by fitting low order polynomials. The object spectrum was modeled by taking the median of the four object spectra extracted from the individual dithered exposures, and smoothing with a  $3 \times 3$  boxcar filter. The model sky and the model galaxy (shifted appropriately for each dithered exposure) were summed to create 2D model spectra, which were subtracted from each exposure. Cosmic rays were identified by comparing the flux in the residual images to the expected noise calculated from the 2D model. Pixels affected by cosmic rays were replaced by the values of corresponding pixels in the model.

Sky lines were subtracted from the cosmic ray cleaned exposures by fitting a third order polynomial in the spatial direction, masking the galaxy and any other objects in the slit. Subtracting the sky lines before wavelength calibration and rectification has the disadvantage that the lines are still slightly tilted. However, the advantage of this procedure is that aliasing due to rectification of sharp, bright lines is avoided; tests showed that such aliasing effects can be avoided entirely by reversing the usual reduction procedure.

A separate wavelength solution was obtained for each of the four galaxy spectra. Arc lamp exposures were taken at regular intervals during the night. A fit to the positions of bright lines in the nearest arc exposure provided the initial solution. The observed locations of the [O I] 5577.34 Å sky line in the blue and the OH 7–3 P1 8885.85 Å sky line in the red were used to correct the zeropoint for each spectrum; these corrections were typically  $\sim 3$  Å. The sky subtracted 2D spectra were transformed to a common  $\log \lambda$  scale.

The galaxy spectra are too faint in individual 1800s exposures for a reliable S-distortion correction. Therefore, the four spectra were first combined into a single 2D spectrum, using linear weighting by the signal-to-noise (S/N) ratio. The S-distortion was removed by binning the spectrum in 100 Å wide bins and fitting a low order polynomial. Atmospheric absorption features were removed using the spectrum of a bright blue star that was included in each of the masks. A long slit spectrum of the star G191B2B (Massey & Gronwall 1990) taken with the same instrumental setup provided an approximate flux calibration. Finally, the six 7200s spectra were combined into a single 43.2 ks spectrum, using optimal weighting.

### 2.3. Spectral Properties

Spectra of the three galaxies that are covered by our *HST* imaging are shown in Fig. 1, smoothed with a boxcar filter of width 10 Å in the observed frame to enhance broad absorption features. The 1D spectra were extracted by summing the five central rows (1''1) in the 2D spectra. No weighting was applied, to facilitate aperture corrections (see § 2.4). For each galaxy the S/N per Å at  $\lambda_{\text{rest}} = 3700$  Å (calculated from the unsmoothed data) is listed in Table 1.

The most prominent absorption features are Ca II H and K, Mg I and Mg II, and the  $\sim 2600$  Å break. Although evolved stellar populations have many absorption features between  $\sim$

3400 Å and  $\sim 3900$  Å, line indices have been defined for only a handful (see Ponder et al. 1998). The strongest are two intrinsically broad lines: a blend at 3580 Å (Davidge & Clark 1994) and a blend of Fe I and Mg I at 3840 Å (Pickles 1985).

Interestingly, galaxies J0848-1 and J0848-2 show [O II] 3727 Å emission, with rest-frame equivalent width  $-17 \pm 2$  Å and  $-13 \pm 2$  Å respectively. Furthermore, all three galaxies show some evidence for enhanced H $\delta$  absorption, although measurements in this spectral region are severely affected by sky line residuals. In galaxy J0848-3 the higher order Balmer lines H $\epsilon$ , H6, and H7 are clearly enhanced as well. H $\epsilon$  and H7 are blended with Ca H and Fe I + Mg I at 3840 Å respectively, but H6 is not contaminated by any strong metal lines. The rest-frame equivalent width of H6 is  $4.5 \pm 0.8$  Å, making J0848-3 the highest redshift “E+A” galaxy (Dressler & Gunn 1983) currently known.

No UV upturn is evident at  $\lambda \lesssim 2500$  Å, consistent with the idea that hot horizontal branch stars do not contribute significantly to the mid-UV flux in stellar population with ages less than  $\sim 5$  Gyr (e.g., Dorman, O’Connell, & Rood 1995; Brown et al. 2000). A full analysis of the mid-UV spectral features is beyond the scope of the present paper; we note here that the mid-UV spectra are very similar to those of nearby galaxies having intermediate age populations, such as NGC 3610 or M32 (see Lotz, Ferguson, & Bohlin 2000).

### 2.4. Velocity Dispersions

Kinematics of nearby early-type galaxies are usually determined from the spectral region containing the strong Mg<sub>b</sub> line at 5172 Å (e.g., Davies et al. 1987; Lucey et al. 1991; Jørgensen, Franx, & Kjaergaard 1995b; Mehlert et al. 2000). Studies of early-type galaxies at  $z \gtrsim 0.5$  have used bluer spectral regions near the G-band at 4300 Å (e.g., van Dokkum & Franx 1996; Kelson et al. 2000a; Koopmans & Treu 2002). Beyond  $z \approx 1.1$  it seems attractive to use the strong Ca II H and K lines for measuring velocity dispersions (see, e.g., Koblunicky & Gebhardt 2000). However, because these lines are intrinsically broad ( $\sigma \approx 5$  Å) they are not very sensitive indicators of velocity dispersion. Additional problems are template mismatch caused by errors in the continuum fitting across the 4000 Å break and the fact that the Ca II H line at 3968 Å is blended with H $\epsilon$  at 3969 Å. Empirically, the Ca II H and K lines appear to overestimate the velocity dispersion (Kormendy & Illingworth 1982).

In the present study we explore the use of near-UV lines blueward of the Ca II H and K lines for measuring velocity dispersions of high redshift galaxies. Central velocity dispersions were determined from a fit to a convolved template star spectrum in real space, following the procedures outlined in van Dokkum & Franx (1996) and Kelson et al. (2000a). The wavelength region is 3400 – 4000 Å in the rest-frame, with regions around [O II] 3727 Å and the Balmer lines masked. The spectra were weighted by the S/N ratio, as determined from sky spectra.

The solar spectrum<sup>5</sup> was used in the fits, because it spans the entire rest-frame wavelength range of our LRIS-R observations at high S/N ratio, and its spectral type is expected to be appropriate for the integrated light of intermediate age stellar populations. The validity of this approach is tested in Sect. 2.5 on two nearby galaxies. For each galaxy the wavelength-dependent instrumental resolution was determined from sky lines, and the solar spectrum was smoothed and rebinned to match the reso-

<sup>5</sup> Obtained from the BAse Solaire Sol 2000 ([http://mesola.obspm.fr/form\\_spectre.html](http://mesola.obspm.fr/form_spectre.html)).

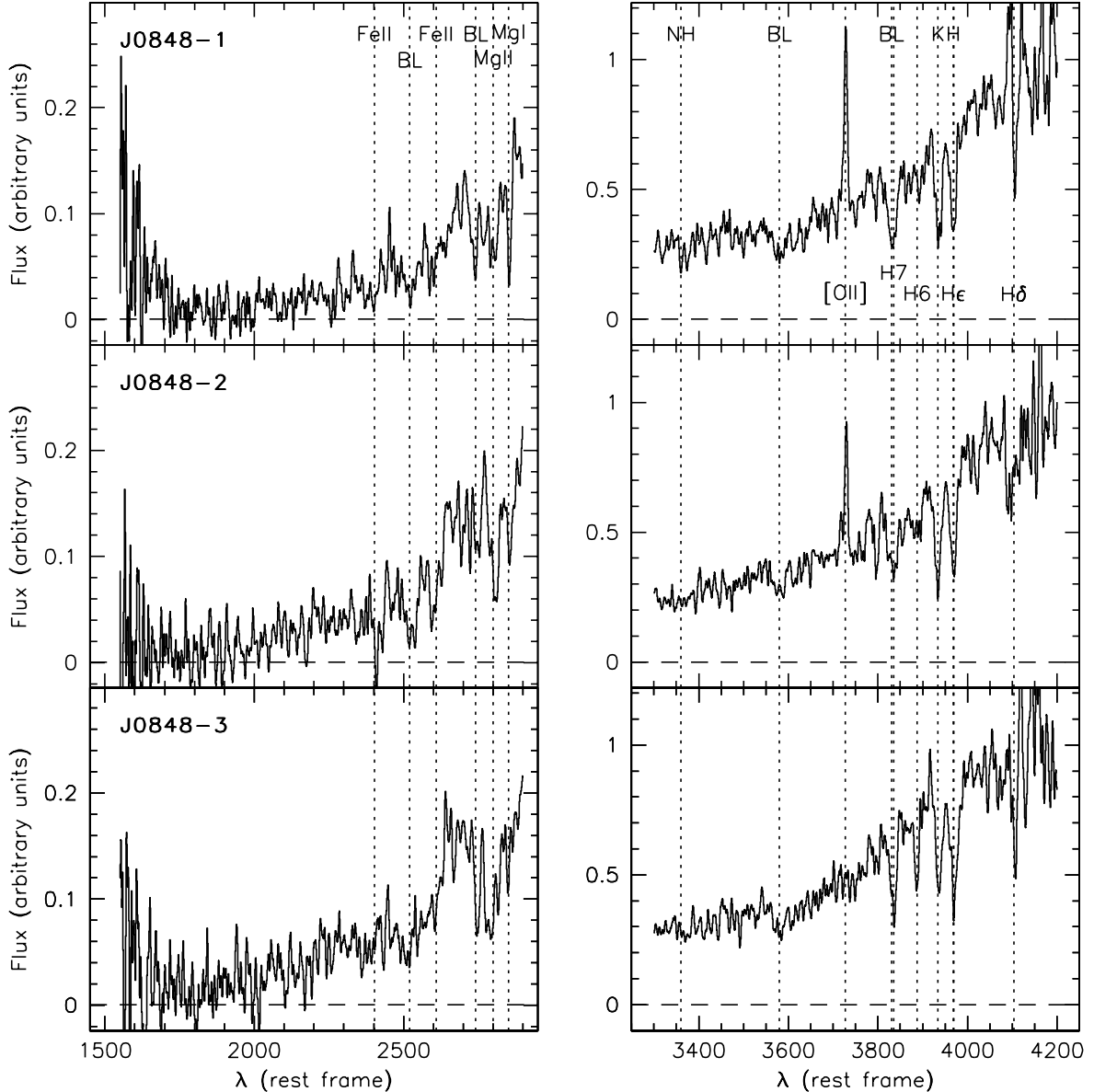


FIG. 1.— Keck spectra of three early-type galaxies in the  $z = 1.27$  cluster RDCS J0848+4453, smoothed by a boxcar filter of width  $10 \text{ \AA}$  in the observed frame. Spectra from the blue arm and the red arm of LRIS are shown separately. The exposure time is 43.2 ks. Galaxies J0848-1 and J0848-2 show [O II] emission; galaxy 0848-3 has strong Balmer absorption lines.

lution of the galaxy spectra.

Fits and their residuals are shown in Fig. 2, and the resulting velocity dispersions are listed in Table 1. For consistency with earlier work the dispersions in our  $0''.9 \times 1''.1$  rectangular apertures were corrected to a circular aperture of  $3''.4$  diameter at the distance of Coma, following the procedure of Jørgensen et al. (1995b). The errors in Table 1 do not include a systematic uncertainty of  $\sim 5\%$ , determined from varying the continuum filtering, the wavelength range, and the weighting scheme. Limiting the fitting range to  $3400 - 3900 \text{ \AA}$  had a negligible effect on the dispersions and their uncertainties, and no stable solutions were found when only the region  $3800 - 4000 \text{ \AA}$  was used in the fit. These results suggest that the Ca II H and K lines have little weight in the fit, as expected from their large intrinsic width.

We were unable to measure stable dispersions when we limited the wavelength range to  $3400 - 3700 \text{ \AA}$ , or split the data in two independent datasets with effective exposure time 21.6 ks. These tests indicate that our observations just reach the required S/N for velocity dispersion measurements at this redshift.

TABLE 1  
VELOCITY DISPERSIONS

Galaxy	S/N	$z$	$\sigma$ ( $\text{km s}^{-1}$ )
J0848-1	14	1.2751	$237 \pm 34$
J0848-2	15	1.2770	$308 \pm 41$
J0848-3	17	1.2774	$174 \pm 29$

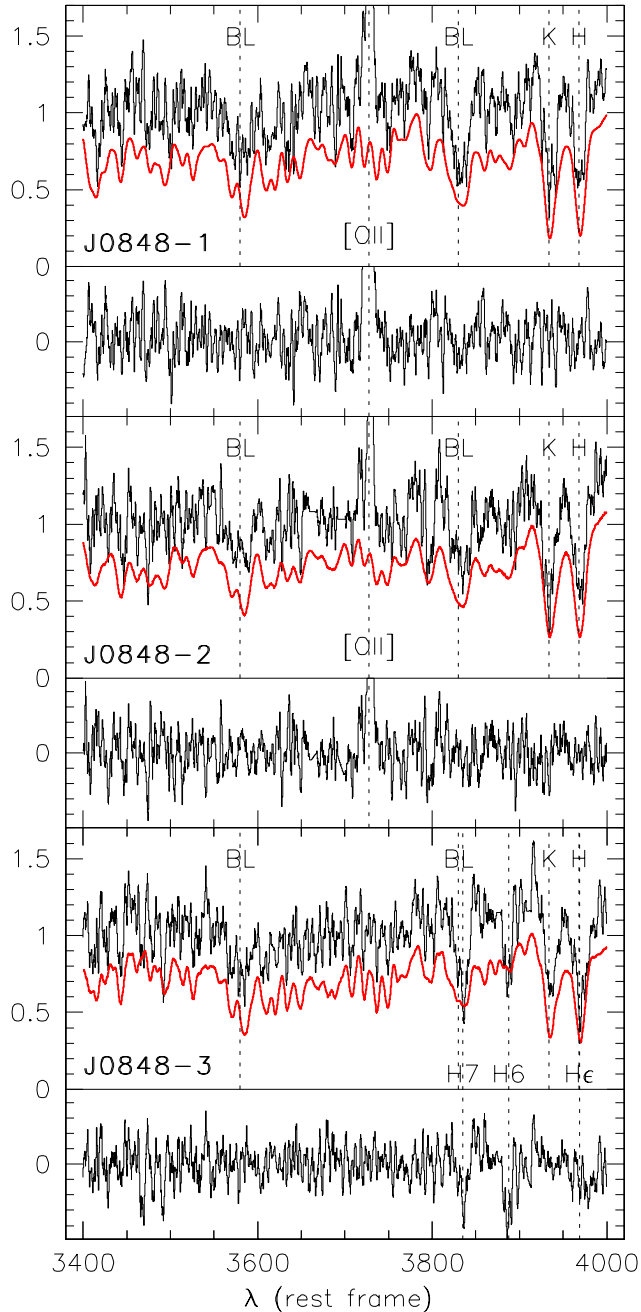


FIG. 2.— The spectral region  $3400 - 4000 \text{ \AA}$  at full resolution, i.e., without any smoothing. The solar spectrum is shown in red, smoothed to the velocity dispersion of the galaxies, and offset for clarity. Below each spectrum the residuals from the fit are shown. Note the higher order Balmer lines in the residuals of J0848-3.

### 2.5. Tests on Two Nearby Galaxies

Moderate resolution near-UV spectra were obtained for two nearby galaxies, NGC 3610 and NGC 5018, in order to test whether velocity dispersions obtained from near-UV lines are unbiased with respect to determinations from redder spectral regions. The galaxies were selected because they are believed to have comparatively young luminosity weighted ages; galaxies at  $z = 1.27$  are at most  $\sim 5$  Gyr old, and their stellar populations may resemble those of young early-type galaxies in the local Universe (see Sect. 2.3).

NGC 3610 is classified as E5, has significant morphological fine structure indicating a recent merger, and is thought to have a centrally concentrated intermediate-age stellar population (Silva & Bothun 1998, and references therein). The galaxy also has a dynamically cold disk (Rix & White 1992). NGC 5018 is an elliptical galaxy with shells, and is also considered to be a recent merger remnant (e.g., Fort et al. 1986). Modelling of line indices indicates the presence of a  $\sim 3$  Gyr old stellar population dominating the light at  $\sim 4000 \text{ \AA}$  (Leonardi & Worthey 2000).

The galaxies were observed 2001 June 19, with the LRIS Double Spectrograph on the Keck I Telescope, using a  $1''.0$  slit and the D460 dichroic. The two arms of LRIS allow simultaneous measurement of velocity dispersions in the red and the near-UV, sampling approximately the same spatial region of the galaxies. The blue arm used the  $1200 \text{ lines mm}^{-1}$  grism blazed at  $3400 \text{ \AA}$ , giving a wavelength range of  $3000 \text{ \AA} - 3800 \text{ \AA}$ . The red arm used the  $900 \text{ lines mm}^{-1}$  grating blazed at  $5500 \text{ \AA}$ ; the grating angle that was used gives a wavelength range of  $4700 - 5950 \text{ \AA}$ . The instrumental resolution as measured from night sky lines  $\sigma_{\text{instr}} \approx 65 \text{ km s}^{-1}$  at  $3500 \text{ \AA}$  and  $\approx 70 \text{ km s}^{-1}$  at  $5200 \text{ \AA}$ . Exposure times were  $1800 \text{ s}$  for NGC 3610 and  $1800 \text{ s}$  for NGC 5018. The observations were done through cirrus and occasional clouds. Spectra of template stars HD 102494 (G9IV), HD 132737 (K0III), and HD 210220 (G6III) were obtained in twilight, using the same instrumental setup.

The reduction followed standard procedures for long slit spectroscopic data. Bias levels were determined from the over-scan regions on the CCD. Internal flat fields were used to correct for the pixel-to-pixel variation of the CCD response. Cosmic rays were removed using the L.A.COSMIC task (van Dokkum 2001). Arc lamp lines were used for wavelength calibration, with zeropoint offsets determined from sky lines in the object spectra. Sky spectra were determined from the edges of the slit, and subtracted. Normalized near-UV spectra of NGC 3610 and NGC 5018 are shown in Fig. 3. The 1D spectra were extracted by summing ten rows, corresponding to  $2''/2$ . The S/N ratio per  $\text{\AA}$  is 55 for NGC 3610 and 23 for NGC 5018. The region  $3465 \text{ \AA} - 3495 \text{ \AA}$  is not shown because the galaxy spectra are severely affected by the presence of an undispersed slit image in that region, caused by insufficient baffling of the blue grism.

Velocity dispersions were determined from a direct fit of the template stars to the galaxy spectra, as discussed in Sect. 2.4. In addition to the three template stars observed with LRIS-B the solar spectrum was used in the fits. The solar spectrum was smoothed and rebinned to match the resolution of the galaxy spectra. The results are listed in Table 2.

There is evidence that the red spectral region gives slightly higher velocity dispersions (by  $\sim 5\%$ ) than the near-UV region. If the effect is real, it may indicate a bias in the measurement technique, or reflect the presence of a dynamically cold component of young stars in these two galaxies. The small difference may also be caused by differential atmospheric refraction (causing misalignment of the slit and the galaxy center in the near-UV), since both galaxies were observed at high airmass. The sign of the difference is consistent with this explanation, but the effect is difficult to quantify because early-type galaxies often show complex structure in their central velocity dispersion profiles (e.g., van der Marel et al. 1994).

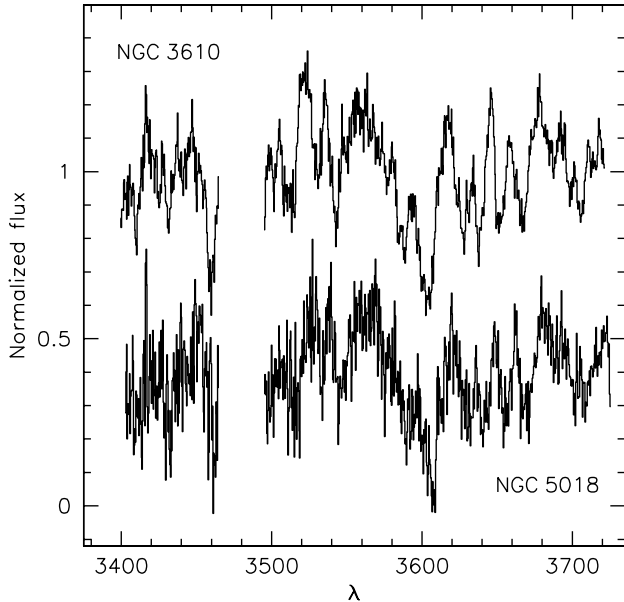


FIG. 3.— Near-UV spectra of NGC 3610 (top) and NGC 5018 (bottom), at a resolution  $\sigma_{\text{instr}} \approx 65 \text{ km s}^{-1}$ . Both spectra were normalized by fitting a low order polynomial; for clarity the spectrum of NGC 5018 was offset by  $-0.6$ . Many moderately strong absorption lines are present in this spectral region. The spectra are significantly affected by stray light in the region  $3465 \text{ \AA} - 3495 \text{ \AA}$ , which is excluded in the velocity dispersion fitting.

The Sun gives very similar results as the other template stars. We conclude that determining velocity dispersions from the near-UV lines using the solar spectrum as a template may introduce systematic errors of  $\sim 5\%$ . Assuming the systematic errors can be added quadratically, we find a total systematic uncertainty of  $\sim 7\%$ .

TABLE 2  
VELOCITY DISPERSIONS OF NEARBY GALAXIES

Galaxy	Template	$\sigma$ ( $M_{\odot}$ )	$\sigma$ (3600)
NGC 3610	HD 102494	$143 \pm 2$	$134 \pm 6$
NGC 3610	HD 132737	$143 \pm 2$	$134 \pm 5$
NGC 3610	HD 210220	$143 \pm 2$	$134 \pm 5$
NGC 3610	Sun	$144 \pm 2$	$135 \pm 6$
NGC 5018	HD 102494	$206 \pm 3$	$199 \pm 15$
NGC 5018	HD 132747	$207 \pm 3$	$197 \pm 15$
NGC 5018	HD 210220	$206 \pm 3$	$199 \pm 15$
NGC 5018	Sun	$206 \pm 3$	$194 \pm 15$

### 3. PHOTOMETRY

Colors and structural parameters were determined from *HST* imaging previously described in van Dokkum et al. (2001b). The cluster was observed in the  $I_{F814W}$  band with the Wide Field and Planetary Camera 2 (WFPC2), and in the  $H_{F160W}$  band with the Near Infra-Red Camera and Multi-Object Spectrometer (NICMOS) NIC3 camera. We refer to van Dokkum et al. (2001b) for details of the observations and reduction. Figure 4 shows a color image of RDCS J0848+4453 created from our *HST* imaging. The pixel scale of our final drizzled images is  $0''.04$ ; the total area covered by both WFPC2 and NICMOS is  $2.3 \text{ arcmin}^2$ .

#### 3.1. Colors

Colors were measured from the  $H_{F160W}$  and  $I_{F814W}$  images in  $1''.5$  diameter apertures, after smoothing the  $I_{F814W}$  images to

the NICMOS resolution. Zeropoints on the Vega system were obtained from the Data Handbooks (STScI, Baltimore) of NICMOS and WFPC2 respectively:

$$H_{F160W} = -2.5 \log(\text{ADU}/s) + 21.496 \quad (1)$$

$$I_{F814W} = -2.5 \log(\text{ADU}/s) + 21.688. \quad (2)$$

A correction of 0.05 magnitudes was applied to the  $I_{F814W}$  zeropoint to account for the long/short anomaly (see, e.g., Wiggs et al. 1998). Galactic extinction is very small in this field ( $E(B - V) \approx 0.02$ ; Schlegel, Finkbeiner, & Davis 1998) and was ignored. Measured colors are listed in Table 3. Errors are estimated at 0.07, dominated by systematic uncertainties in the zeropoints.

TABLE 3  
PHOTOMETRY

Galaxy	$K_s$ Total	$I_{814}$ $r < 0''.75$	$I_{814} - H_{160}$ $r < 0''.75$	$\log r_e$ "	$\mu_{e,160}$
J0848-1	17.36	22.90	3.48	$-0.010$	21.75
J0848-2	17.97	22.94	3.35	$-0.460$	20.19
J0848-3	18.71	22.85	3.10	$-0.880$	18.49

#### 3.2. Structural Parameters

Following the procedures outlined in van Dokkum & Franx (1996) effective radii and effective surface brightnesses were determined for the three galaxies with measured velocity dispersions. For each galaxy, models consisting of an  $r^{1/4}$  law convolved with a Point Spread Function (PSF) were fitted directly to the two-dimensional images. The NICMOS  $H_{F160W}$  images were used in the fits, because the galaxies have much higher S/N than in the WFPC2  $I_{F814W}$  images. Furthermore effects of color gradients are minimized by fitting in the rest-frame  $R$ -band rather than the rest-frame  $U$ -band.

A separate PSF was used for each galaxy. The PSFs were created by applying the same dither pattern as used in the observations to model PSFs generated by Tiny Tim (Krist 1995). The PSFs were then combined and rebinned using “drizzle” (Fruchter & Hook 1997), in the same way as the observations. We note that our results are not very sensitive to errors in the PSFs or color gradients, because the error in the product  $r_e I_e^{0.83}$  is almost parallel to the FP (see, e.g., Jørgensen, Franx, & Kjærgaard 1995a). Results from the fits are listed in Table 3. Effective radii are in arcseconds; surface brightnesses are in  $H_{F160W} \text{ mag/arcsec}^2$  and not corrected for  $(1+z)^4$  cosmological dimming.

For a meaningful comparison between galaxies at different redshifts, measured surface brightnesses need to be converted to a common rest-frame band. We assume that the flux density in the rest-frame  $B$  band can be related to the flux density in the observed  $I_{F814W}$  and  $H_{F160W}$  bands by  $F_{B(z)} = F_I^\alpha F_H^{1-\alpha}$  (see van Dokkum & Franx 1996). Using spectral energy distributions from Coleman, Wu, & Weedman (1980) we find for  $z = 1.27$

$$B_z = H_{F160W} + 0.50(I_{F814W} - H_{F160W}) + 1.81 \quad (3)$$

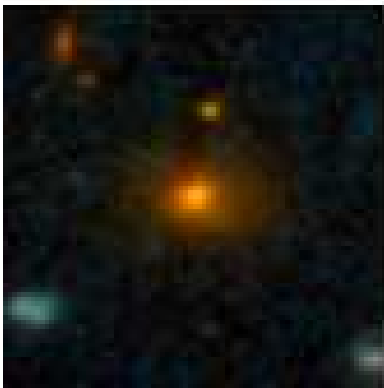
and, similarly,

$$R_z = H_{F160W} + 0.02(I_{F814W} - H_{F160W}) + 1.95, \quad (4)$$

with the subscript  $z$  denoting rest-frame (i.e., redshifted) band. These transformations are very different from a traditional  $K$ -correction, as they use the observed colors of the galaxies to interpolate between passbands. As a result, they are independent of spectral type to  $\sim 0.03 \text{ mag}$ . The total systematic error



J0848-1



J0848-2



J0848-3



FIG. 4.— Color rendition of the core of RDCS J0848+4453 at  $z = 1.27$ , created from a WFPC2  $I_{F814W}$  image and a mosaic of three *HST* NICMOS  $H_{F160W}$  images. The WFPC2 data were smoothed and resampled to match the resolution of the NICMOS data. Most of the objects appearing orange are cluster members. The insets show the three early-type galaxies with measured velocity dispersions. The scale of the large image is  $2'.23 \times 2'.23$ , and of the insets  $10'' \times 10''$ .

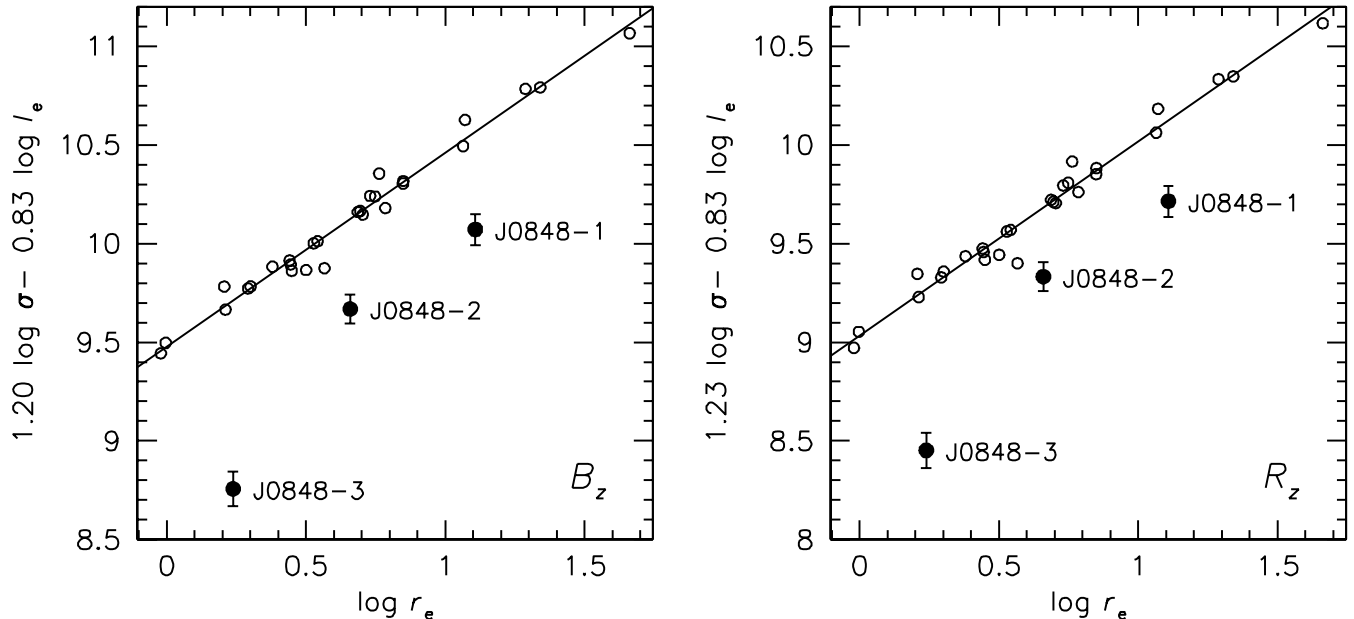


FIG. 5.— Edge-on projection of the Fundamental Plane of the nearby Coma cluster (Jørgensen et al. 1996) in the  $B$  and  $R$  bands (open symbols). Solid symbols show the three early-type galaxies at  $z = 1.27$ . Surface brightnesses were corrected for  $(1+z)^4$  cosmological dimming, and transformed to the rest-frame  $B$  and  $R$  bands;  $\log I_e \equiv -0.4\mu_e$ . The  $z = 1.27$  galaxies are offset with respect to the FP of Coma due to passive evolution of the stellar populations. The offsets are larger in the rest-frame  $B$  band than in the rest-frame  $R$  band. In both bands the offset is greatest for the “E+A” galaxy J0848-3. More data are needed to determine the form of the FP at  $z = 1.27$ .

is estimated at  $\sim 0.05$ , which includes uncertainties in absolute spectrophotometry (see, e.g., van Dokkum & Franx 1996). Note that the redshifted Cousins  $R$  filter is a close match to the observed  $H_{F160W}$  filter.

As a test on our entire procedure we also determined structural parameters from the WFPC2  $I_{F814W}$  images, using Tiny Tim PSFs and Eq. 3 to convert surface brightnesses to the  $B_z$  band. We find that the difference in the parameter  $r_e I_e^{0.83}$  is 5% for J0848-1, 8% for J0848-2, and 16% for J0848-3. Given the much higher S/N in the NICMOS images these results can be viewed as upper limits to the true uncertainties. We conclude that the uncertainties in the  $M/L$  ratios of individual galaxies are dominated by random errors in the velocity dispersions.

#### 4. FUNDAMENTAL PLANE AND MASS-TO-LIGHT RATIOS

The velocity dispersions and structural parameters allow us to study the Fundamental Plane of early-type galaxies at  $z = 1.27$ . The Fundamental Plane of nearby clusters has the form

$$r_e \propto \sigma^\alpha I_e^\beta \quad (5)$$

with  $I_e$  surface brightness at the effective radius in linear units. Jørgensen, Franx, & Kjærgaard (1996) find  $\alpha = 1.20$ ,  $\beta = -0.83$  in the  $B$ -band and  $\alpha = 1.23$ ,  $\beta = -0.83$  in Gunn  $r$  from an analysis of 225 early-type galaxies in ten nearby clusters. Assuming that early-type galaxies form a homologous family, the observed tilt of the FP implies that the  $M/L$  ratios of galaxies scale with their mass as

$$M/L \propto M^{0.28} r_e^{-0.07} \quad (6)$$

in the  $B$  band. Therefore, the evolution of the Fundamental Plane tracks the evolution of the  $M/L$  ratios of galaxies (Franx 1995).

#### 4.1. Edge-on Projection of the Fundamental Plane

In Fig. 5 open symbols show the edge-on projection of the FP of the nearby Coma cluster (Jørgensen et al. 1996), and solid symbols show the three galaxies in RDCS J0848+4453 at  $z = 1.27$ . The Jørgensen et al. Gunn  $r$  data were transformed to Cousins  $R$  using  $R - r = 0.35$  (Fukugita, Shimasaku, & Ichikawa 1995). Surface brightnesses were corrected for  $(1+z)^4$  cosmological dimming. All three galaxies show a large offset from the FP of Coma, and we conclude that the galaxies at  $z = 1.27$  do not occupy the same Fundamental Plane as Coma galaxies. The offsets are smaller in the  $R_z$  band than in the  $B_z$  band, consistent with the expectation that early-type galaxies at  $z = 1.27$  are bluer than those in Coma. Galaxies J0848-1 and J0848-2 show a much smaller offset than the E+A galaxy J0848-3.

Our sample of three galaxies is obviously too small to determine the coefficients  $\alpha$  and  $\beta$ . The tilt of the FP may evolve with time due to various processes, such as systematic age differences between low mass galaxies and high mass galaxies. A study of 30 early-type galaxies in the cluster CL 1358+62 at  $z = 0.33$  has shown that the form of the FP has not changed significantly over the past  $\sim 4$  Gyr (Kelson et al. 2000b). At higher redshift the samples are still too small to place strong constraints on the tilt. In the following, we do not strictly assume that the form of the FP at  $z = 1.27$  is the same as in nearby clusters, but we do assume that offsets from the Coma FP are due to changes in  $M/L$  ratio resulting from stellar evolution. This interpretation is supported by the fact that the E+A galaxy shows the largest deviation, and it is consistent with the reduced offsets in  $R_z$  compared to  $B_z$ .



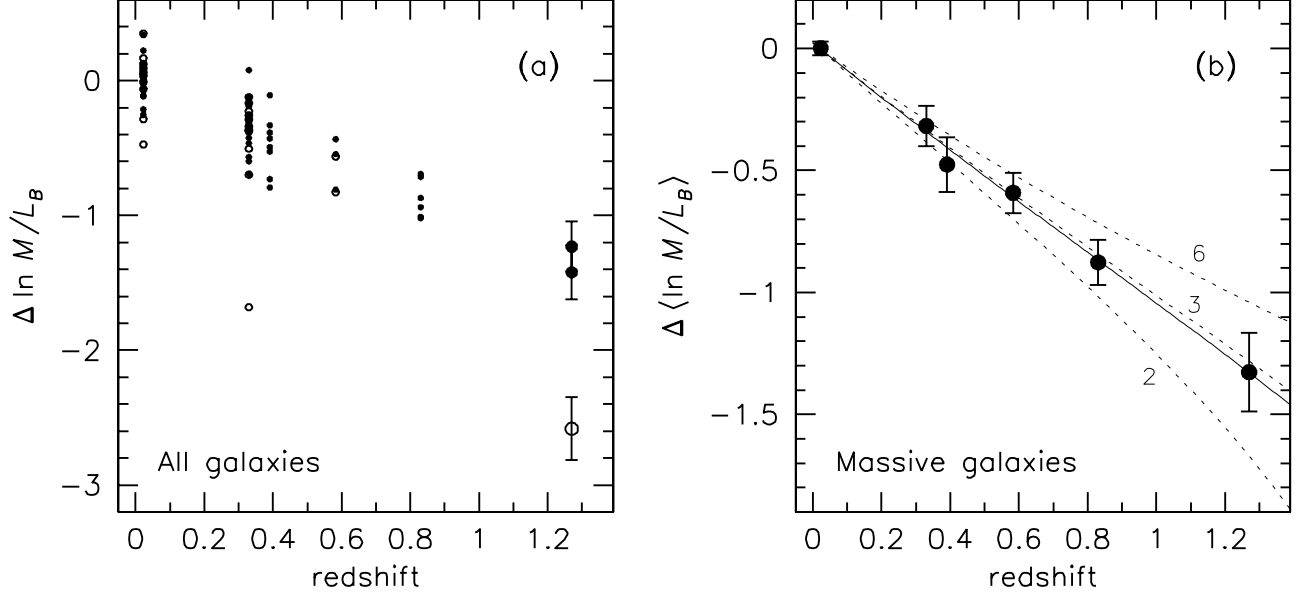


FIG. 6.— Evolution of the  $M/L$  ratio of early-type cluster galaxies, in the rest-frame  $B$  band. In (a) individual galaxies in clusters at  $0.02 \leq z \leq 1.27$  are shown. Data at  $z < 1$  are taken from Jørgensen et al. 1996, van Dokkum et al. (1998) and Kelson et al. (2000). Open symbols are galaxies with masses  $M < 10^{11} M_{\odot}$ . In (b) the data for each cluster are averaged, excluding galaxies with masses  $M < 10^{11} M_{\odot}$ . Broken lines are predictions from simple single burst stellar population synthesis models, with  $z_{\text{form}} = 6, 3,$  and  $2$ . The solid line is a prediction from models incorporating morphological evolution, taken from van Dokkum & Franx (2001). The  $M/L$  ratios of the two most massive galaxies in RDCS J0848+4453 are consistent with an extrapolation of results obtained at  $z < 1$ .

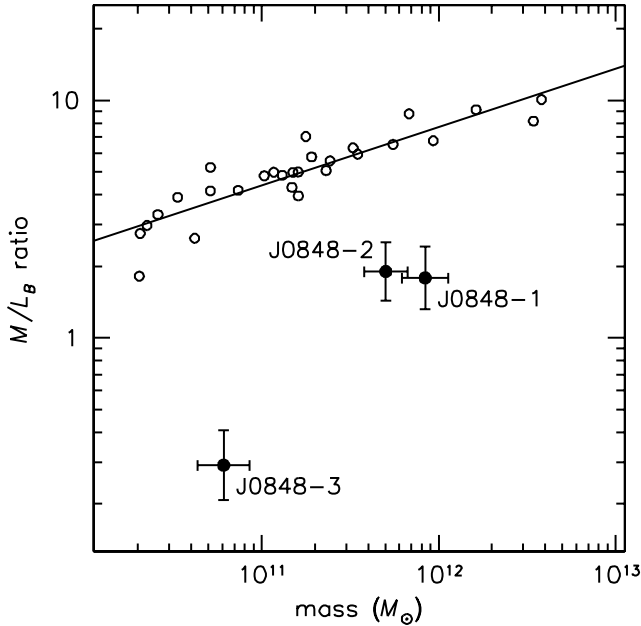


FIG. 7.— Rest-frame  $B$  band mass-to-light ratio versus mass, for galaxies in Coma (open circles) and RDCS J0848+4453 (solid circles). Galaxy J0848-3, the galaxy with the largest offset from Coma (i.e., the youngest stellar population), is a factor  $\sim 10$  less massive than J0848-1 and J0848-2.

#### 4.2. Evolution of Mass-to-Light Ratios

The evolution of the mean  $M/L$  ratio can be determined directly from the evolution of the zeropoint of the FP (see Eq. 6 and van Dokkum & Franx 1996). Similarly, for a single

galaxy the offset from the Coma FP can be expressed as an offset in  $M/L$  ratio. Offsets for individual galaxies in clusters at  $0.02 \leq z \leq 1.27$  are shown in Fig. 6(a). The offsets in  $\ln M/L_B$  for galaxies J0848-1 and J0848-2 are  $-1.37 \pm 0.15$  and  $-1.27 \pm 0.14$  respectively, remarkably consistent with an extrapolation of results obtained at  $0.02 \leq z \leq 0.83$ . The offset of J0848-3 is much larger at  $\Delta \ln M/L_B = -2.58 \pm 0.17$ , corresponding to a factor  $\approx 13$ .

In Fig. 7 we investigate the  $M/L$  ratios of galaxies in RDCS J0848+4453 in more detail by showing the projection of the FP on the  $M/L$  ratio vs. mass plane. These quantities are defined in a straightforward way:

$$\log M \equiv 2 \log \sigma + \log r_e + C_1 \quad (7)$$

and

$$\log M/L_B \equiv 2 \log \sigma - \log I_e - \log r_e + C_2. \quad (8)$$

With  $\log I_e \equiv -0.4(\mu_{e,B} - 27.0)$ ,  $r_e$  in kpc,  $C_1 = 6.07$  and  $C_2 = -1.29$ , mass and  $M/L$  ratio are expressed in solar units (see Jørgensen et al. 1996).

The mass of galaxy J0848-3 is a factor  $\sim 10$  lower than that of J0848-1 and J0848-2, and similar to the lowest mass galaxies in the Jørgensen et al. (1996) Coma sample. We conclude that its inclusion in our small sample is probably due to its high surface brightness and low  $M/L$  ratio, and it is unlikely (although not impossible) that this object is representative for galaxies in the mass range  $10 < \log M < 11$ .

In Fig. 6 (b) we show the evolution of the mean  $M/L$  ratio of high mass galaxies, by selecting objects with  $M > 10^{11} M_{\odot}$  in all clusters (solid symbols in Fig. 6a). Note that this is not a true mass selected sample, since we may miss “underluminous” galaxies with very high  $M/L$  ratios. The evolution is remarkably uniform and linear over the entire redshift range  $0.02 \leq z \leq 1.27$ . A linear fit gives  $\ln M/L_B \propto (-1.06 \pm 0.09)z$ ,

with the error dominated by systematic uncertainties. The rms scatter around the best fitting relation is only 0.03, significantly smaller than expected from the uncertainties in the individual datapoints. This may partly be caused by the cancellation of systematic errors, but can also be the result of small number statistics. This is almost certainly true for RDCS J0848+4453 itself, because the random errors in the velocity dispersions alone already introduce an uncertainty of  $\sim 13\%$  in the average offset of J0848-1 and J0848-2.

#### 4.3. Implications for Luminosity Weighted Ages

The evolution of the mean  $M/L$  ratio depends on the slope of the Initial Mass Function (IMF), the metallicity, cosmological parameters, and the luminosity weighted age of the stellar population (see, e.g., Tinsley & Gunn 1976; Worthey 1994). Furthermore, the observed evolution needs to be corrected for the effects of morphological evolution (van Dokkum & Franx 2001). The cited studies provide a comprehensive discussion of these issues, beyond the scope of the present paper. Here we only consider two models: a simple model with a fixed IMF, varying age, and no morphological evolution, and the best fitting complex model from van Dokkum & Franx (2001).

##### 4.3.1. Simple Models

In Fig. 6(b) the dotted lines show predictions of simple models with a Salpeter (1955) IMF, Solar metallicity, and a range of formation redshifts. The models are of the form  $L \propto (t - t_{\text{form}})^{\kappa}$ , with  $\kappa$  determined from stellar population synthesis models (see van Dokkum et al. 1998, and references therein). The formal best fitting formation redshift is  $z_* = 2.6_{-0.4}^{+0.9}$ , corresponding to a luminosity weighted age of  $\sim 2$  Gyr at the epoch of observation. Note that these results do not apply to the low mass galaxy J0848-3, which has a much lower luminosity weighted age of  $\sim 0.5$  Gyr. This age is qualitatively consistent with the presence of strong Balmer absorption lines in its spectrum.

The new data reinforce earlier studies at lower redshift. Interestingly the formal error in the formation redshift of the stars in massive galaxies suggests an upper limit of  $z_* = 3.5$  ( $1\sigma$ ), whereas previous studies could only provide lower limits. However, as discussed in van Dokkum et al. (1998) the inferred formation redshifts are strongly dependent on the assumed cosmology and IMF.

##### 4.3.2. Complex Models

The models discussed so far implicitly assume that early-type galaxies in high redshift clusters are typical progenitors of present-day early-type galaxies. However, there is good evidence that the set of early-type galaxies evolves with time. Dressler et al. (1997) and others (e.g., van Dokkum et al. 2001b; Lubin, Oke, & Postman 2002) have found a gradual decrease with redshift of the fraction of early-type galaxies in clusters, from  $\sim 80\%$  in low redshift clusters to  $\sim 45\%$  in clusters at  $z \sim 1$ , suggesting that  $\sim 50\%$  of early-type galaxies was transformed from other galaxy types in the last half of the age of the Universe.

A consequence of such morphological evolution is that the sample of early-type galaxies at  $z = 1.3$  is only a subset of the full sample of progenitors of present-day early-type galaxies. Furthermore, the subset is biased, consisting of the oldest progenitors. As a result the observed evolution of early-type galaxies underestimates the true evolution that would be measured if all progenitors had been accounted for. van Dokkum

& Franx (2001) developed analytical models which take this ‘‘progenitor bias’’ into account. They can be used to correct the ages of early-type galaxies for the effects of morphological evolution. As shown in van Dokkum & Franx (2001) a model with progenitor bias can provide excellent simultaneous fits to the observed evolution of the mean  $M/L$  ratio, the early-type galaxy fraction, and the scatter in the color-magnitude relation at  $0.02 \leq z \leq 0.83$ . Their best fitting model is shown by the solid line in Fig. 6(b). In this model the mean luminosity weighted formation redshift of the stars in all present-day early-type galaxies  $\langle z_* \rangle = 2.0_{-0.2}^{+0.3}$ , whereas the formation redshift of the stars in the subset of early-type galaxies that were already assembled at  $z = 1.27$  is higher, at  $\langle z_* \rangle \approx 2.5$ . As can be seen in Fig. 6(b) the fit is equally good as simple models with  $z_* \approx 3$ .

In summary, the  $M/L$  ratios of the two galaxies with masses  $> 10^{11} M_{\odot}$  are well fitted by extrapolations of models fitted to data at  $z < 1$ . Good fits are obtained for simple models that ignore selection effects and also for self-consistent models which incorporate morphological evolution.

## 5. CORRECTING FOR LUMINOSITY EVOLUTION AT $z \approx 1.3$

The observed evolution of the  $M/L$  ratio can be used directly to correct the luminosities of distant galaxies for passive evolution, and convert luminosity to mass. Ultimately measurements of  $M/L$  ratios at high redshift should remove the need for stellar population synthesis models to interpret the evolution of the luminosity function, and provide a direct measurement of the evolution of the galaxy mass function. The logarithmic correction we derive from massive cluster galaxies at  $0.02 \leq z \leq 1.27$  corresponds to a brightening of  $1.50 \pm 0.13$  magnitudes at  $z = 1.3$ . In absolute terms, a typical early-type galaxy with  $M/L_B = 5.9 h_{50}$  in units of  $(M/L_B)_{\odot}$  in the local Universe (van der Marel 1991) has  $M/L_B = 1.5 \pm 0.2 h_{50}$  at  $z = 1.3$ .

Massive early-type galaxies are expected to be a minor contributor to  $K$ -selected samples of high redshift galaxies (e.g., Cimatti et al. 2002), but they may form a large fraction of the population of Extremely Red Objects. In Fig. 8 the distance from the Coma Fundamental Plane, expressed in  $R_z$  magnitudes, is plotted against  $I - H$  color. Interestingly, despite the low  $M/L$  ratio of J0848-3 all three galaxies have  $I - H > 3$  (and also  $R - K > 5$ ) and fall in the class of Extremely Red Objects. As discussed in § 4.3 simple models with  $z_{\text{form}} \approx 3$  can be used to correct galaxies J0848-1 and J0848-2 for luminosity evolution, but such models severely underpredict the required correction for J0848-3. Since EROs are usually not selected by mass but on the basis of  $K$ -band luminosity, ERO samples cannot be pruned by applying a mass cut (as we did in § 4.2 for galaxies with measured kinematics). Therefore, we conclude from our small sample that it is hazardous to use simple ‘‘Passive Luminosity Evolution’’ (PLE) models (e.g., Pozzetti et al. 1996) to correct EROs for luminosity evolution. Our results show that the correction can range from 1 – 2.5 magnitudes in the  $H$ -band at  $z \approx 1.3$ , even in a restricted sample of luminous EROs with early-type morphology. We note that it may be possible to improve the reliability of the correction by including a color term (for galaxies of known redshift); as demonstrated in Fig. 8 the observed correlation between  $\Delta H$  and  $I - H$  color is similar to the expected correlation from stellar population synthesis models.

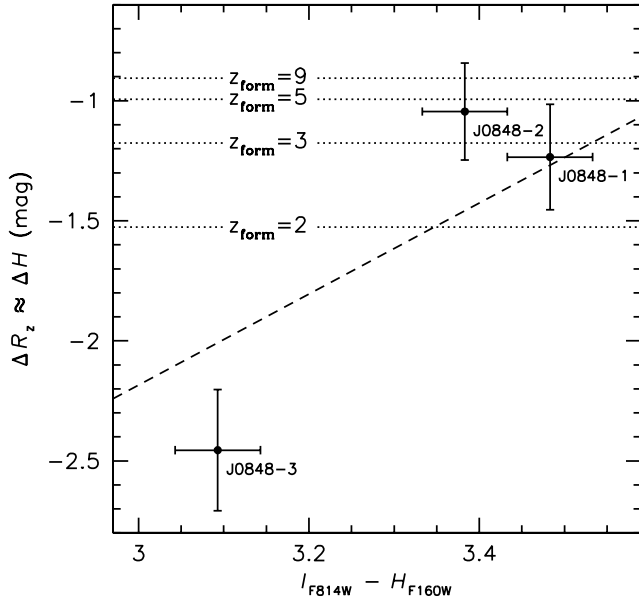


FIG. 8.— Correction for luminosity evolution in rest-frame  $R$  (approximately observed  $H$ ) for the three early-type galaxies at  $z = 1.27$ . All three galaxies have  $I - H > 3$ , and fall in the class of “Extremely Red Objects”. Predicted corrections for different formation redshifts of the stars are indicated by dotted lines. The dashed line indicates the expected relation between rest-frame  $U - R$  color and  $R$  magnitude for a Salpeter (1955) IMF, solar metallicity, and varying age. Simple “PLE” models with  $z_{\text{form}} \approx 3$  accurately predict the observed luminosity evolution for two galaxies, but underpredict the luminosity evolution of J0848-3 by more than a magnitude.

## 6. CONCLUSIONS

We have presented results on the Fundamental Plane of early-type galaxies in the cluster RDCS J0848+4453 at  $z = 1.27$ . Although our sample of three galaxies cannot be used for a determination of the tilt and scatter in the FP, we can interpret the  $M/L$  ratios of individual galaxies by comparing them to the prediction of the FP in local clusters. The  $M/L$  ratios of the two most massive galaxies, when combined with those of massive galaxies in clusters at  $0.02 \leq z \leq 0.83$ , are consistent with a very regular evolution of the mean  $M/L$  ratio of the form  $\ln M/L_B \propto (-1.06 \pm 0.09)z$ . The third galaxy is a factor  $\sim 10$  less massive than the other two, and has a much lower  $M/L$  ratio. Our data are insufficient to determine whether the  $M/L$  ratio of this galaxy is typical for its mass. It is clear, however, that it is due to the presence of a young stellar population: the galaxy has an “E+A” spectrum, and its relatively blue color is consistent with its low  $M/L$  ratio. Unfortunately it will be diffi-

cult to obtain much larger samples in a single cluster at  $z \sim 1.3$ , although it may be possible to combine results from different clusters to constrain the evolution of the FP better.

The overall conclusion from our work on RDCS J0848+4453 is that by  $z \sim 1.3$  we are approaching the epoch of formation of massive cluster galaxies. In van Dokkum et al. (2001b) we have shown that the most luminous galaxies show signs of interactions, with the second brightest cluster galaxy (a merger of three red  $\sim L_*$  galaxies) the most spectacular example. Furthermore, we presented evidence that the slope of the color-magnitude relation may be flatter than in low redshift clusters. The present paper shows that the spectra of three of the most luminous early-type galaxies indicate the presence of a young stellar population in one galaxy, and possibly residual ongoing star formation in the other two. Furthermore, their  $M/L$  ratios indicate luminosity weighted ages of only 0.5 – 2 Gyr at the epoch of observation.

As discussed in § 5 the measurements presented here are relevant in a broader context than the evolution of galaxies in clusters, as they can be used to correct the luminosities of distant red galaxies for passive evolution of their stellar populations. Ultimately measurements of the Fundamental Plane and Tully-Fisher relation at high redshift, when combined with measurements of the luminosity function, should lead to an empirical determination of the evolution of the mass function. The sparse observations that are available now are already valuable, since they can be used to calibrate stellar population synthesis models and provide realistic errors estimates. Apart from collecting larger samples in high redshift clusters, an obvious next step is to obtain similar data on field galaxies to determine whether there is an environmental dependence.

We thank Mark Dickinson and Chris Hanley for the NICMOS reductions, and Brad Holden for help with the PSFs. The detailed comments of the anonymous referee improved the text. P. G. v. D. acknowledges support by NASA through Hubble Fellowship grant HF-01126.01-99A awarded by the Space Telescope Science Institute, which is operated by the Association of Universities for Research in Astronomy, Inc., for NASA under contract NAS 5-26555, and through the SIRTFF Fellowship Program, administered by the California Institute of Technology. S. A. S. is supported by the Institute of Geophysics and Planetary Physics (operated under the auspices of the US Department of Energy by the UC Lawrence Livermore National Laboratory under contract W-7405-Eng-48), and by NASA/LTSA grant NAG5-8430. The authors wish to extend special thanks to those of Hawaiian ancestry on whose sacred mountain we are privileged to be guests. Without their generous hospitality, many of the observations presented herein would not have been possible.

## REFERENCES

- Bender, R., Saglia, R. P., Ziegler, B., Belloni, P., Greggio, L., Hopp, U., & Bruzual, G. 1998, *ApJ*, 493, 529  
 Brown, T. M., Bowers, C. W., Kimble, R. A., & Ferguson, H. C. 2000, *ApJ*, 529, L89  
 Cimatti, A., et al. 2002, *A&A Letters*, in press (astro-ph/0207191)  
 Cole, S., Lacey, C. G., Baugh, C. M., & Frenk, C. S. 2000, *MNRAS*, 319, 168  
 Coleman, G. D., Wu, C.-C., & Weedman, D. W. 1980, *ApJS*, 43, 393  
 Cowie, L. L., Songaila, A., Hu, E. M., & Cohen, J. G. 1996, *AJ*, 112, 839  
 Daddi, E., Cimatti, A., & Renzini, A. 2000, *A&A*, 362, L45  
 Davidge, T. J. & Clark, C. C. 1994, *AJ*, 107, 946  
 Davies, R. L., Burstein, D., Dressler, A., Faber, S. M., Lynden-Bell, D., Terlevich, R. J., & Wegner, G. 1987, *ApJS*, 64, 581  
 Djorgovski, S. & Davis, M. 1987, *ApJ*, 313, 59  
 Dorman, B., O’Connell, R. W., & Rood, R. T. 1995, *ApJ*, 442, 105  
 Dressler, A. & Gunn, J. E. 1983, *ApJ*, 270, 7  
 Dressler, A., Lynden-Bell, D., Burstein, D., Davies, R. L., Faber, S. M., Terlevich, R., & Wegner, G. 1987, *ApJ*, 313, 42  
 Dressler, A., Oemler, A., Jr., Couch, W. J., Smail, I., Ellis, R. S., Barger, A., Butcher, H., Poggianti, B. M., & Sharples, R. M. 1997, *ApJ*, 490, 577  
 Drory, N., Bender, R., Snigula, J., Feulner, G., Hopp, U., Maraston, C., Hill, G. J., & de Oliveira, C. Mendes, 2001, *ApJ*, 562, L111  
 Eggen, O. J., Lynden-Bell, D., & Sandage, A. R. 1962, *ApJ*, 136, 748  
 Ferreras, I. & Silk, J. 2001, *ApJ*, 557, 165  
 Fort, B. P., Prieur, J.-L., Carter, D., Meatheringham, S. J., & Vigroux, L. 1986, *ApJ*, 306, 110  
 Franx, M. 1993, *PASP*, 105, 1058

- Franx, M. 1995, in IAU Symp. 164: Stellar Populations, Vol. 164, 269
- Fruchter, A. & Hook, R. N. 1997, in Proc. SPIE Vol. 3164, Applications of Digital Image Processing XX, Andrew G. Tescher, Ed., Vol. 3164, 120
- Fukugita, M., Shimasaku, K., & Ichikawa, T. 1995, PASP, 107, 945
- Holden, B. P., Stanford, S. A., Rosati, P., Squires, G., Tozzi, P., Fosbury, R. A. E., Papovich, C., Eisenhardt, P., et al. 2001, AJ, 122, 629
- Jimenez, R., Friaca, A. C. S., Dunlop, J. S., Terlevich, R. J., Peacock, J. A., & Nolan, L. A. 1999, MNRAS, 305, L16
- Jørgensen, I., Franx, M., & Kjærgaard, P. 1995a, MNRAS, 273, 1097
- . 1995b, MNRAS, 276, 1341
- . 1996, MNRAS, 280, 167
- Kauffmann, G. & Charlot, S. 1998, MNRAS, 297, L23
- Kelson, D. D., Illingworth, G. D., van Dokkum, P. G., & Franx, M. 2000a, ApJ, 531, 159
- . 2000b, ApJ, 531, 184
- Kelson, D. D., van Dokkum, P. G., Franx, M., Illingworth, G. D., & Fabricant, D. 1997, ApJ, 478, L13
- Kobulnicky, H. A. & Gebhardt, K. 2000, AJ, 119, 1608
- Koopmans, L. V. E. & Treu, T. 2002, ApJ Letters, submitted (astro-ph/0201017)
- Kormendy, J. & Illingworth, G. 1982, ApJ, 256, 460
- Krist, J. 1995, in ASP Conf. Ser. 77: Astronomical Data Analysis Software and Systems IV, Vol. 4, 349
- Leonardi, A. J. & Worthey, G. 2000, ApJ, 534, 650
- Lotz, J. M., Ferguson, H. C., & Bohlin, R. C. 2000, ApJ, 532, 830
- Lubin, L. M., Oke, J. B., & Postman, M. 2002, AJ, 124, 1905
- Lucey, J. R., Guzman, R., Carter, D., & Terlevich, R. J. 1991, ApJ, 253, 584
- Massey, P. & Gronwall, C. 1990, ApJ, 358, 344
- McCarthy, P. J., et al. 2001, ApJ, 560, L131
- Mehlert, D., Saglia, R. P., Bender, R., & Wegner, G. 2000, A&AS, 141, 449
- Oke, J. B., et al. 1995, PASP, 107, 375
- Pickles, A. J. 1985, ApJS, 59, 33
- Ponder, J. M., Burstein, D., O'Connell, R. W., Rose, J. A., Frogel, J. A., Wu, C., Crenshaw, D. M., Rieke, M. J., et al. 1998, AJ, 116, 2297
- Pozzetti, L., Bruzual A., G., & Zamorani, G. 1996, MNRAS, 281, 953
- Rix, H. & White, S. D. M. 1992, MNRAS, 254, 389
- Roche, N. D., Almaini, O., Dunlop, J., Ivison, R. J., & Willott, C. J. 2002, MNRAS, in press (astro-ph/0205259)
- Rosati, P., Stanford, S. A., Eisenhardt, P. R., Elston, R., Spinrad, H., Stern, D., & Dey, A. 1999, AJ, 118, 76
- Salpeter, E. E. 1955, ApJ, 121, 161
- Schlegel, D. J., Finkbeiner, D. P., & Davis, M. 1998, ApJ, 500, 525
- Searle, L., Sargent, W. L. W., & Bagnuolo, W. G. 1973, ApJ, 179, 427
- Silva, D. R. & Bothun, G. D. 1998, AJ, 116, 2793
- Somerville, R. S., Primack, J. R., & Faber, S. M. 2001, MNRAS, 320, 504
- Stanford, S. A., Elston, R., Eisenhardt, P. R., Spinrad, H., Stern, D., & Dey, A. 1997, AJ, 114, 2232
- Stanford, S. A., Holden, B., Rosati, P., Tozzi, P., Borgani, S., Eisenhardt, P. R., & Spinrad, H. 2001, ApJ, 552, 504
- Stern, D., Connolly, A., Eisenhardt, P., Elston, R., Holden, B., Rosati, P., Stanford, S. A., Spinrad, H., et al. 2001, in Deep Fields, 76
- Tinsley, B. M. & Gunn, J. E. 1976, ApJ, 203, 52
- Treu, T., Stiavelli, M., Casertano, S., Moller, P., & Bertin, G. 1999, MNRAS, 308, 1037
- . 2002, ApJ, 564, L13
- Tully, R. B. & Fisher, J. R. 1977, A&A, 54, 661
- van der Marel, R. P. 1991, MNRAS, 253, 710
- van der Marel, R. P., Rix, H. W., Carter, D., Franx, M., White, S. D. M., & de Zeeuw, T. 1994, MNRAS, 268, 521
- van Dokkum, P. G. 2001, PASP, 113, 1420
- van Dokkum, P. G. & Franx, M. 1996, MNRAS, 281, 985
- . 2001, ApJ, 553, 90
- van Dokkum, P. G., Franx, M., Kelson, D. D., & Illingworth, G. D. 1998, ApJ, 504, L17
- . 2001a, ApJ, 553, L39
- van Dokkum, P. G. & Stanford, S. A. 2001, ApJ, 562, L35
- van Dokkum, P. G., Stanford, S. A., Holden, B. P., Eisenhardt, P. R., Dickinson, M., & Elston, R. 2001b, ApJ, 552, L101
- Vogt, N. P., Forbes, D. A., Phillips, A. C., Gronwall, C., Faber, S. M., Illingworth, G. D., & Koo, D. C. 1996, ApJ, 465, L15
- Vogt, N. P., Phillips, A. C., Faber, S. M., Gallego, J., Gronwall, C., Guzman, R., Illingworth, G. D., Koo, D. C., et al. 1997, ApJ, 479, L121
- White, S. D. M. & Frenk, C. S. 1991, ApJ, 379, 52
- Wiggs, M. S., Casertano, S., Whitmore, B. C., Mutchler, M., Biretta, J. A., & WFPC2 Photometry Team 1998, BAAS, 30, 1298
- Worthey, G. 1994, ApJS, 95, 107
- Ziegler, B. L., Böhm, A., Fricke, K. J., Jäger, K., Nicklas, H., Bender, R., Drory, N., Gabasch, A., et al. 2002, ApJ, 564, L69